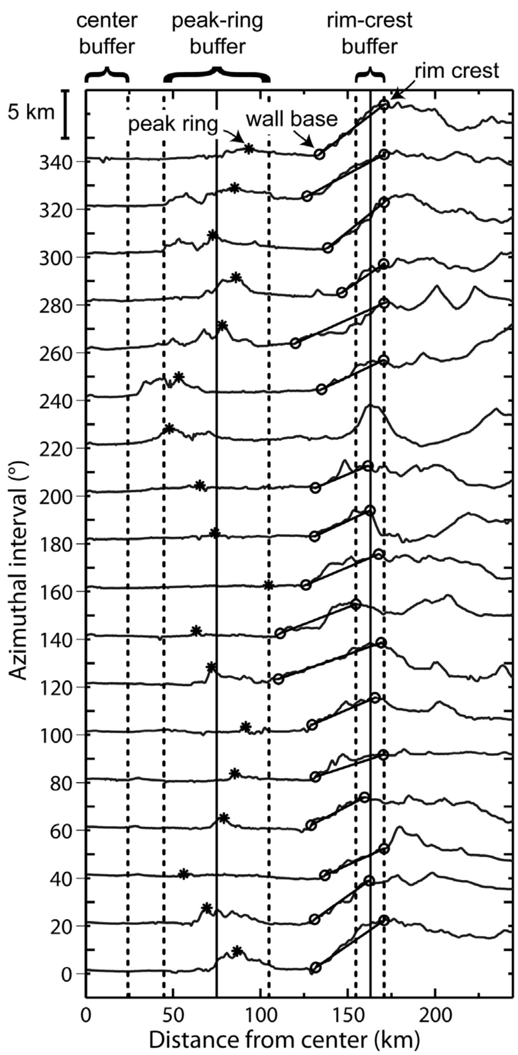

Figure 4. Radial topographic profiles at 20° azimuthal intervals for Schrödinger basin, shown out to 1.5 times the basin radius (244.5 km). The locations of each profile track are shown in Figure 3, with 0° azimuth defining north and increasing azimuth in the clockwise direction. The limits of the center, peak-ring, and rim-crest buffer zones (Figure 3a) are given as vertical dashed lines, with the location of the rim-crest diameter and ring diameter as measured by *Baker et al.* [2011a] given as solid vertical lines. Also shown are the locations of the peak-ring (asterisk, *), wall-base (open circle), and rim-crest (open circle) reference points determined within each buffer zone. The solid line connecting the wall-base and rim-crest reference points represent the reference line used to estimate the wall slope. No wall-base and rim-crest reference points are given for the profile at 220° azimuth, due to an exclusion zone over this interval (Figure 3b).

4.1. The Basin Catalog

[15] Peak-ring basins and protobasins under study are from the catalogs of *Baker et al.* [2011a], which include measurements of the basins' rim-crest, peak-ring, and central peak (for protobasins) diameters along with the central coordinates of a circle fit to the rim crest. To filter the most degraded basins from our topographic analysis, these basins of *Baker et al.* [2011a] were first qualitatively classified based on their degradation state on a scale of I to IV, with IV being the most degraded and I being the morphologically freshest basins (Table 1). These classifications were based on the number of superposed craters and the completeness and degree of erosion of the rim crest and walls. Only those basins with degradation classes of I or II were included in the analysis, which includes 8 of 17 peak-ring basins and 3 of 3 protobasins in the catalogs of *Baker et al.* [2011a] (Table 1).

[16] We also examined the general geology of the protobasins and peak-ring basins using LRO Wide-angle Camera (WAC) mosaics at 100 m/pixel resolution [*Robinson et al.*, 2010] and previous lunar geological maps [*Wilhelms and El-Baz*, 1977; *Lucchitta*, 1978; *Stuart-Alexander*, 1978; *Wilhelms et al.*, 1979], in order to identify possible effects of mare infill on the topography of basins. Three peak-ring basins (Schrödinger, Moscoviense, and Apollo) and two of the three protobasins (Antoniadi and Compton) have mare or mare-like material within their interiors [*Stuart-Alexander*, 1978; *Wilhelms et al.*, 1979; *Haruyama et al.*, 2009; *Mest et al.*, 2010]. Although some of the topographic characteristics of these basins, especially basin depths, have certainly been modified by this infilling, the preservation of prominent peak-ring topography and low areal extent of the mare material in most of the basins suggest that modification has been very limited compared to other mare-filled basins where peak rings and other interior landforms have been completely covered. For example, the most recent estimates for mare thicknesses in Mare Orientale in the Orientale basin, which also preserves much of its original topography, are on order of ~200 m [*Whitten et al.*, 2011], less than previous estimates [e.g., *Head*, 1982]. With the preservation of peak-ring topography and the smaller diameters of peak-ring basins and protobasins, it is unlikely that mare material thicknesses in these basins are much greater than a few hundred of meters. While mare infilling is certainly affecting our measurements, several hundred meters of mare fill is well below the already inherent kilometer-scale topographic variation in the rim-crest topography (see Figure 5). As such, we did not exclude those basins that have been partially infilled with mare from our topographic analysis. Two basins, Schrödinger and Compton, exhibit fracture patterns that crosscut all floor units and peak-ring material and bear resemblance to some floor-fractured craters [*Schultz*, 1976]. Based on the proposed mechanism for how floor fractures occur in these craters [*Schultz*, 1976], it is possible that Compton and Schrödinger could have experienced post-impact uplift of their floors that could modify our topographic calculations. Upon analysis of multiple topographic profiles across their floors, we find little evidence of doming that may have initiated fracturing of their interiors. However, it is noted that Compton appears to have an anomalously small depth compared to other protobasins (see section 5.1). While this may be a product of the floor-fracturing process, it may also represent an important geometric variation in the transition from complex craters to peak-ring basins or a product of varying impact conditions (see section 5.1). For these reasons, we therefore chose to include both Schrödinger and Compton in our analysis.